CHEMISTRY OF MATERIALS

ARTICLE

pubs.acs.org/cm

Combined Neutron and Synchrotron X-ray Diffraction Investigation of the $BaCe_{0.85-x}Zr_xY_{0.15}O_{3-\delta}$ ($0.1 \leq x \leq 0.4$) Proton Conductors

Lorenzo Malavasi,*[,†] Cristina Tealdi,[†] Clemens Ritter,[‡] Vladimir Pomjakushin,[§] Fabia Gozzo,[∥] and Yuri Diaz-Fernandez[†]

[†]Dipartimento di Chimica Fisica "M. Rolla", INSTM (UdR Pavia) and IENI-CNR, Università di Pavia, Viale Taramelli 16, 27100 Pavia, Italy

[‡]Institute Laue-Langevin, Boite Postale 156, F-38042, Grenoble, France

[§]Laboratory for Neutron Scattering, ETHZ and PSI, CH-5232, Villigen PSI, Switzerland

[∥]Swiss Light Source, 5232 Villigen PSI, Switzerland

ABSTRACT: In this paper we investigated, by means of combined neutron and X-ray synchrotron diffraction, the structural properties of the $BaCe_{0.85-x}Zr_xY_{0.15}O_{3-\delta}$ solid solution as a function of Zr-doping ($0.1 \leq x \leq 0.4$) and temperature. Compositions within this system have been proposed as electrolytes for intermediate temperature solid oxide fuel cells (IT-SOFC) due to their significant proton conductivities. However, no systematic investigations of the crystal structure evolution as a function of temperature have been reported in the literature. In this paper, we could define the phase stability up to 800 °C for each member of the $BaCe_{0.85-x}Zr_xY_{0.15}O_{3-\delta}$ solid solution showing that for lower Zr-doping levels (x = 0.1 and 0.2) four different crystal structures are found in the T-range investigated. For higher Zr-doping levels (x = 0.3 and 0.4), the samples show a more symmetric structure already at room temperature (rhombohedral symmetry) and pass through two phase transitions. The exact knowledge of the structural features as a function of temperature is an essential piece of information in order to assess the possible use of these electrolyte materials in real devices.

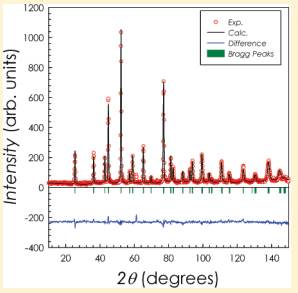

KEYWORDS: proton conductors, neutron diffraction, thermal analysis, electrical conductivity

INTRODUCTION

A major worldwide challenge is the development of cleaner, sustainable sources of energy to deal with the environmental threat of global warming and the finite nature of fossil fuel reserves.[1] One leading technology for future power generation is the solid oxide fuel cell (SOFC). SOFCs are of particular interest because of their high efficiency (compared to combustion-based technologies), low emissions, and fuel flexibility; the latter allows them to use hydrocarbon fuels and hence act as a bridging technology between hydrocarbon- and future hydrogen-based economies.[1−5] They usually operate between 800 and 1000 °C, and the available operating temperature range strongly depends on the characteristics of the anode, cathode, and electrolyte materials. Target ionic conductivities for the electrolyte at operating temperatures are typically ≥0.1 S cm^{-1}. One important challenge in improving SOFC technology is to reduce the working temperature to 500−700 °C. Such intermediate-temperature SOFCs would hasten implementation of this technology in distributed combined heat and power (CHP) systems.[1−5] In addition, lowering the working temperature is advantageous in terms of long-term operation, materials stability, cost, and safety.

Solid state proton conductors are attractive candidates for applications in intermediate-temperature solid oxide fuel cells (IT-SOFCs). In fact, proton conducting electrolytes for IT-SOFCs have also the advantage of water production at the cathode, thus avoiding the fuel dilution at the anode. The first report of high-temperature proton conductivity in an oxide material dates back to the 1980s when Iwahara and co-workers observed this phenomenon in doped strontium and barium cerates.[6,7] After more than 20 years of active research, the perovskite-type cerates and zirconates have become well-established proton conducting systems.[8−21] The crystal structures of these materials are based on the perovskite structure with different degrees of distortion as a function of composition and temperature.

Protonic defects are formed by the dissociative absorption of water at the surface, which requires the presence of oxide-ion vacancies. Water from the gas-phase dissociates into a hydroxide ion and a proton, with the hydroxide ion filling an oxide-ion vacancy and the proton forming a covalent bond with a lattice oxygen. In Kröger−Vink notation, this reaction can be written

$$H_2O_g + V_O^{\bullet\bullet} + O_O^X \leftrightarrow 2OH_O^{\bullet} \quad (1)$$

Pure $SrCeO_3$, $BaCeO_3$, $CaZrO_3$, and $SrZrO_3$ exhibit only low proton incorporation unless doped with subvalent cations. In the $BaCeO_3$ system, for example, replacing Ce^{4+} ions with M^{3+} cations (typically Y^{3+}) is charge-compensated by formation of oxygen vacancies:

$$2Ce_{Ce}^X + Y_2O_3 + O_O^X \rightarrow 2Y'_{Ce} + V_O^{\bullet\bullet} + 2CeO_2 \quad (2)$$

Among the proton-conducting oxides investigated so far, barium cerate ceramics show high proton conductivity, particularly when

Received: December 1, 2010
Revised: January 17, 2011
Published: February 03, 2011

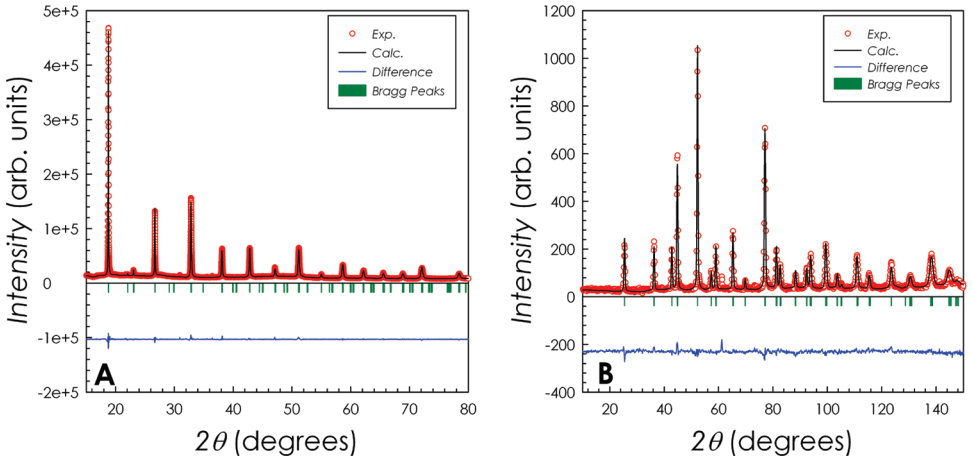

Figure 1. Rietveld refined synchrotron X-ray (A) and neutron (B) diffraction patterns for $BaCe_{0.55}Zr_{0.30}Y_{0.15}O_{3-\delta}$ at room temperature: observed, calculated, difference profile, and Bragg peaks.

Table 1. Structural Data at Room Temperature for the $BaCe_{0.85-x}Zr_xY_{0.15}O_3$ Solid Solution

		$x = 0.1$	$x = 0.2$	$x = 0.3$	$x = 0.4$
space group		$I2/m$	$I2/m$	$R\bar{3}c$	$R\bar{3}c$
a (Å)		6.217 81(4)	6.179 93(4)	6.137 62(2)	6.091 27(6)
b (Å)		8.712 99(7)	8.6927(6)	6.137 62(2)	6.091 27(6)
c (Å)		6.194 22(6)	6.17599(4)	14.993 6(3)	14.917 0(8)
β (deg)		90.510 6(6)	90.3893(6)		
V (Å^3)		335.563(5)	331.770(5)	489.146(3)	479.32(7)
Ba	x	0.255 9(6)	0.259 5(6)	0	0
	y	0	0	0	0
	z	0.740 2(9)	0.727(1)	0.25	0.25
	B	0.89(6)	1.04(8)	0.41(2)	0.74(2)
Ce/Y	x	0.25	0.25	0	0
	y	0.25	0.25	0	0
	z	0.25	0.25	0	0
	B	0.81(6)	0.82(7)	0.62(2)	0.47(2)
O1	x	0.226 2(7)	0.185 8(8)	0.4420(4)	0.460 9(4)
	y	0	0	0	0
	z	0.248 9(7)	0.225 0(8)	0.25	0.25
	B	2.16(7)	2.97(8)	1.42(2)	1.36(2)
	occ	1.00(2)	0.99(2)	0.975(4)	0.980(4)
O2	x	0	0		
	y	0.321(1)	0.278(1)		
	z	0	0		
	B	3.34(8)	3.7(1)		
	occ	1.01(2)	1.00(2)		
O3	x	0.5	0.5		
	Y	0.213 9(9)	0.225(1)		
	z	0	0		
	B	3.08(8)	3.90(8)		
	occ	0.94(2)	0.92(2)		
R_{wp}, χ^2		6.5, 2.34	4.53, 2.11	5.05, 3.13	4.28, 1.74

doped with 15 or 20% of Y, reaching values around $10^{-2}\ \Omega^{-1}\ cm^{-1}$ at 600 °C.[6,7] As a drawback, the chemical stability of doped $BaCeO_3$ for fuel cell applications is lacking. In particular, in hydrocarbon- or syngas-fueled SOFCs, barium cerates easily react in a CO_2-containing atmosphere and can decompose into barium carbonate and cerium oxide at temperatures below 800 °C. The chemical stability of doped barium zirconates is far greater.[22,23] Although there is high intrinsic proton mobility in $BaZrO_3$, which is cubic at room temperature,[24] the conductivity of polycrystalline samples is often significantly lower than the bulk because of large grain boundary resistance. Perovskite

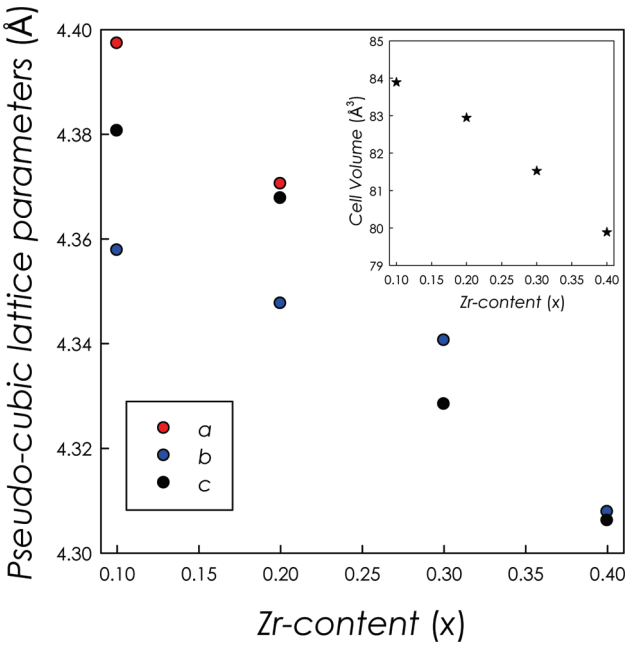

Figure 2. Pseudocubic lattice parameters and cell volume at room temperature as a function of Zr-content for the $BaCe_{0.85-x}Zr_xY_{0.15}O_{3-\delta}$ solid solution. Error bars are smaller than the symbols.

cerates and zirconates are mutually soluble, so to develop electrolytes with adequate proton conductivity and good chemical stability under conditions typically encountered during fuel cell operation, cerate–zirconate solid solutions are being investigated.[14,22,23,25−27]

In recent years several papers dealt with the preparation and conductivity study of the $BaCe_{1-x-y}Zr_xY_yO_{3-\delta}$ solid solution.[22,23,28,29] Problems related to the sintering of such compositions have been overcome by means of wet-chemistry preparation routes[23] leading to significant bulk proton conductivities comparable to those of doped barium cerates. In addition, for $y = 0.15$ the cerates/zirconates become stable against barium carbonate formation for $x \geq 0.15$.[23]

On the other hand, the knowledge of the structural properties of the $BaCe_{1-x-y}Zr_xY_yO_{3-\delta}$ solid solution as a function of Zr-doping and temperature is lacking. All the available reports deal with room

dx.doi.org/10.1021/cm1034326 |Chem. Mater. 2011, 23, 1323–1330

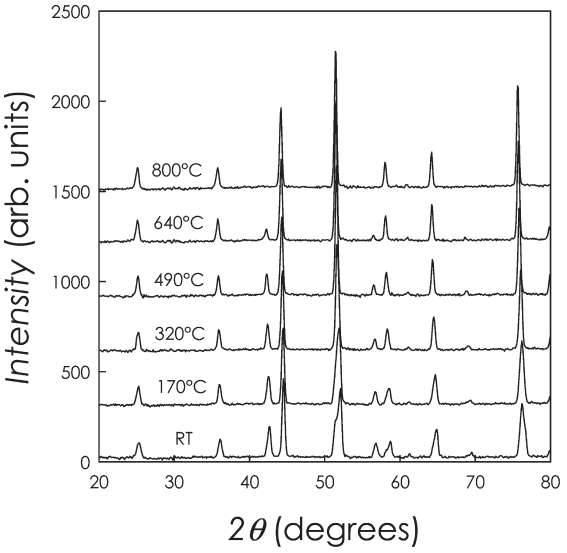

Figure 3. Fragment of the neutron diffraction patterns (D1A. ILL, λ = 1.9085 Å) as a function of temperature collected on the $BaCe_{0.75}Zr_{0.10}Y_{0.15}O_{3-\delta}$ sample.

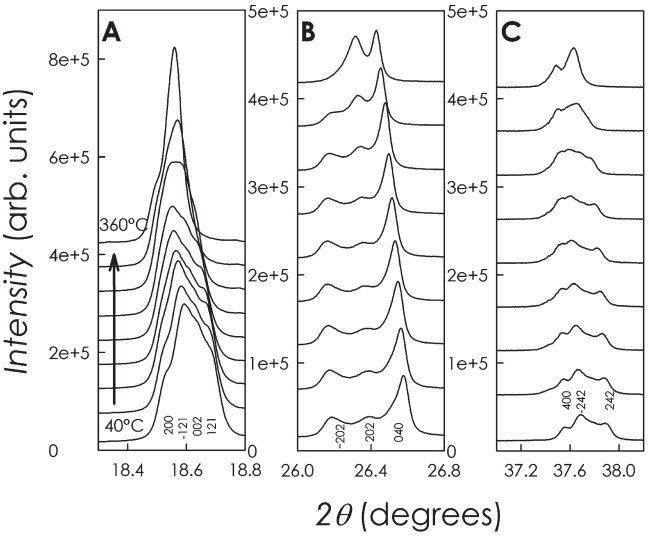

Figure 4. Synchrotron X-ray diffraction patterns, at selected 2θ regions, as a function of temperature (40 °C < T < 360 °C) for $BaCe_{0.75}Zr_{0.10}Y_{0.15}O_{3-\delta}$.

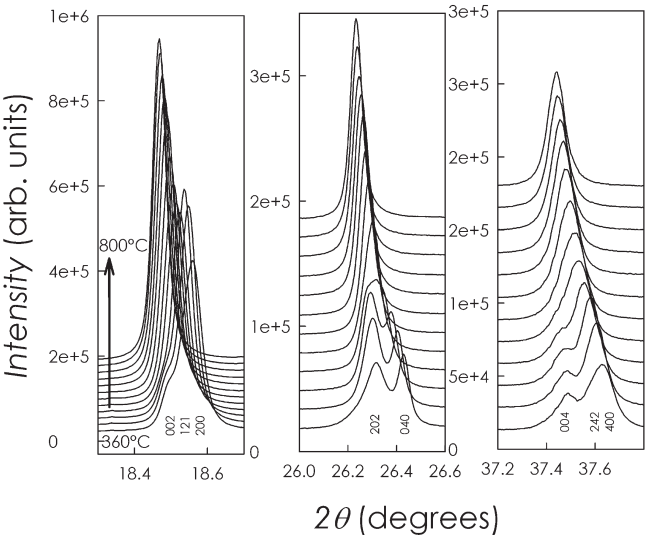

Figure 5. Synchrotron X-ray diffraction patterns, at selected 2θ regions, as a function of temperature (360 °C < T < 800 °C) for $BaCe_{0.75}Zr_{0.10}Y_{0.15}O_{3-\delta}$.

temperature data collected on laboratory X-ray diffractometers. However, as it is well-known, changes in the perovskite symmetry can be subtle and difficult to be observed with low-quality diffraction data. In addition, the structural evolution as a function of temperature in the range of operation is not known. However, such a piece of information is essential when thinking of incorporating an electrolyte material into a device. We have recently[30] carried out a thorough structural investigation of the $BaCe_{0.80}Y_{0.20}O_{2.9}$ proton conducting oxide which, despite being one of the most studied compositions, was not known for what concerns its behavior as a function of temperature. The diffraction results allowed us to define the evolution of the crystal structure of $BaCe_{0.80}Y_{0.20}O_{2.9}$ as a function of temperature revealing that (a) from RT to 400 it is monoclinic with space group $I2/m$; (b) at 500 °C the materials adopts the orthorhombic *Imma* structure; (c) at 600 and 700 °C it is rhombohedral ($R\bar{3}c$); and (d) finally at 800 °C it becomes cubic ($Pm\bar{3}m$). This work showed the importance of following the structural evolution of cerates in order to properly correlate their physical properties (i.e., conductivity) with the phase changes as a function of temperature.[30]

In the present paper we are going to present the experimental investigation, realized by means of high-resolution neutron and synchrotron X-ray diffraction data, on the $BaCe_{0.85-x}Zr_xY_{0.15}O_{3-\delta}$ solid solution as a function of Zr-doping ($0.1 \leq x \leq 0.4$) and temperature. This Y-content has been chosen since it corresponds to the highest proton conductivity and easier proton solubility.[6,7,15]

EXPERIMENTAL SECTION

Powder samples of $BaCe_{0.85-x}Zr_xY_{0.15}O_{3-\delta}$ solid solution ($0.1 \leq x \leq 0.4$) have been prepared by conventional solid state reaction from the proper stoichiometric amounts of $BaCO_3$, CeO_2, ZrO_2, and Y_2O_3 (all Aldrich ≥99,9%) by two successive firings for 20 h at 1200 °C. X-ray diffraction analysis carried out on a Bruker D8 Advance diffractometer (Cu radiation, 2θ-range 10−110°, step size 0.02°, time per step 5 s) was used for assessment of phase purity of the as synthesized material. No traces of spurious phases have been detected. The chemical composition was checked by means of microprobe analysis which revealed a sample composition in agreement with the nominal one.

Neutron powder diffraction data were acquired on the D1A instrument at the Institute Laue Langevin (ILL) in Grenoble and on HRPT[31] at PSI (Villigen, Zurich). All measurements were recorded in static air in a silica glass container at ILL and in a V container at PSI. The neutron diffraction patterns were collected in the angular range 0°−160°, step 0.05° at a wavelength 1.9085 Å (ILL) and 1.494 Å (PSI) in the temperature range between room temperature and 750 or 800 °C every 100 °C.

All the neutron diffraction patterns were analyzed according to the Rietveld method by means of the FULLPROF software package.[32] Cell parameters, atomic positions, and isotropic thermal factors for all the cations and anisotropic thermal factors for oxygens were refined. The background coming from the empty quartz tube was recorded at the same temperatures and subtracted from the NPD patterns of the samples for the data collected at ILL.

The high-temperature (30−750 °C) X-ray powder diffraction (XRPD) measurements have been carried out at the Swiss Light Source

dx.doi.org/10.1021/cm1034326 |*Chem. Mater.* 2011, 23, 1323–1330

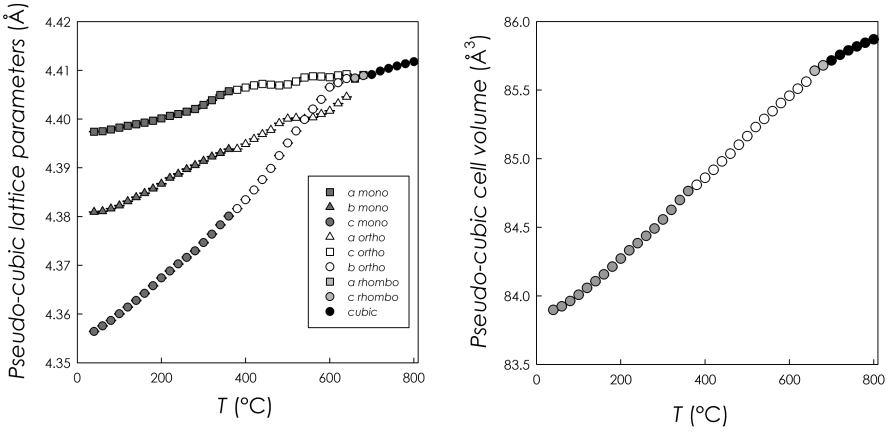

Figure 6. Trend of lattice parameters and unit cell volume as a function of temperature for the $BaCe_{0.75}Zr_{0.10}Y_{0.15}O_{3-\delta}$ sample.

Materials Science beamline powder diffraction station. The samples were loaded in quartz capillaries in a STOE furnace, and the measurements were carried out at ambient pressure, approximately every 20 °C. Full diffraction patterns (60°) were collected using the fast Mythen microstrip detector at a wavelength of 1.001 085 Å, as determined using a standard silicon powder (NIST 640c).[33]

3. RESULTS AND DISCUSSION

3.1. Crystal Structure Evolution at Room Temperature as a Function of Zr-Content. Room temperature data have been analyzed by means of a combined Rietveld refinement of synchrotron X-ray and neutron diffraction data. Such an approach showed to be essential in order to correctly define the crystal structure of the $BaCe_{0.85-x}Zr_xY_{0.15}O_{3-\delta}$ solid solution. The perovskite structure is known to possess a range of distortions which can lower the symmetry from the ideal cubic cell to rhombohedral, orthorhombic, and monoclinic symmetry. Such distortions are related to octahedral tiltings which progressively increase from the cubic to the monoclinic structure. For example, in the monoclinic structure (space group, s.g., $I2/m$), found at room temperature in the $BaCe_{0.85}Y_{0.15}O_{3-\delta}$ compound,[30] one is facing a two-tilt system known, in the Glazer's notation[34] as $a^\circ b^- c^-$; in the orthorhombic *Imma* space group the tilt around the *z*-axis is the same as around the *y*-axes ($a^\circ b^- b^-$) and one is in a two-tilt system as well. The rhombohedral symmetry ($R\bar{3}c$) removes one tilting bringing the symmetry of the system to the $a^- a^- a^-$ tilt system, i.e., the rotation angle is the same about each of the three axes with rotations of two neighboring octahedra, along the tilt axis, which are in opposite directions. Finally, the cubic $Pm\bar{3}m$ space group is described as a $a^\circ a^\circ a^\circ$ tilt system which excludes any tilting between octahedra.

Some of these distortions are revealed in the diffraction patterns as very subtle peak splittings and/or peak broadenings. With common laboratory X-ray diffraction it might not be possible to distinguish or reveal, for example, the presence of a very small monoclinic distortion. So, high resolution X-ray diffraction is needed in these cases. On the other hand, the use of neutron diffraction helps strongly in the phase identification if the difference between two structures is found in few low-intensity superlattice peaks originating from the tilting of the oxygen sublattice.

Figure 1 shows, as a selected example, the refined X-ray and neutron patterns for the $x = 0.3$ member of the $BaCe_{0.85-x}Zr_xY_{0.15}O_{3-\delta}$ solid solution. Table 1 reports the room temperature (RT) structural data for the four samples investigated

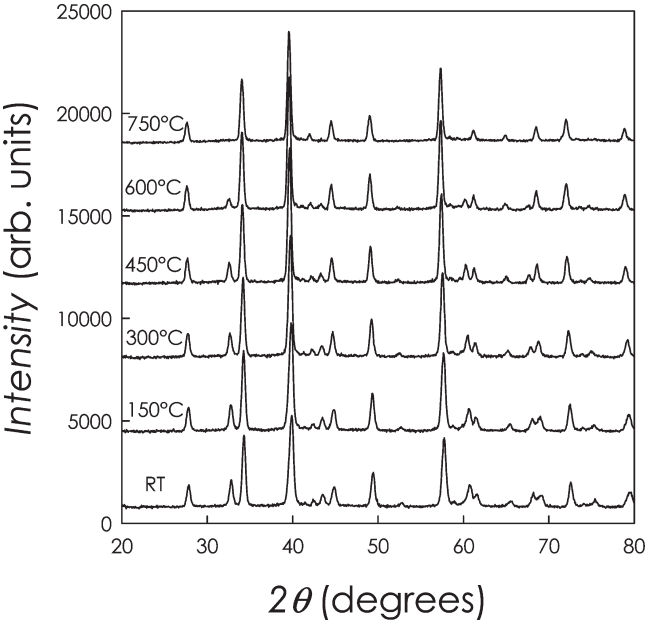

Figure 7. Fragment of the neutron diffraction patterns (D1A. ILL, λ = 1.9085 Å) as a function of temperature collected on the $BaCe_{0.65}Zr_{0.20}Y_{0.15}O_{3-\delta}$ sample.

obtained by means of a combined refinement of X-ray and neutron diffraction data. As can be seen, with an increase of the Zr content, the structure becomes more symmetric at room temperature. $x = 0.1$ and 0.2 members of the $BaCe_{0.85-x}Zr_xY_{0.15}O_{3-\delta}$ solid solution have a monoclinic cell (s.g., $I2/m$) with the monoclinic distortion decreasing by increasing the Zr amount (β angle moves toward 90°). $x = 0.3$ and 0.4 samples have a rhombohedral unit cell. In addition, the cell contracts along with the Zr-doping as expected due to the smaller ionic radius of Zr^{4+} (0.86 Å) with respect to Ce^{4+} (1.01 Å) for the same coordination. Refinement of the O-atoms occupancy showed that, within the estimated standard deviation, the samples have an oxygen deficiency which correlates quite well with the level of vacancies induced by the Y-doping. Refined values of the oxygen site(s) occupancies are reported in Table 1. According to these refinements, it seems that for the monoclinic structure, where three oxygen sites are present, the tendency is toward finding vacancies mainly on the O3 site. From the oxygen occupancies it turned out

dx.doi.org/10.1021/cm1034326 |*Chem. Mater.* 2011, 23, 1323–1330

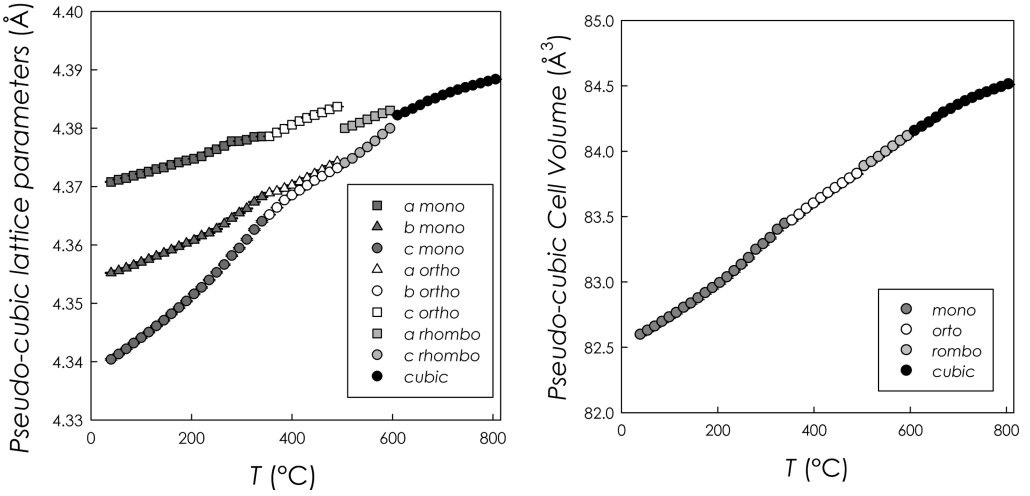

Figure 8. Trend of lattice parameters and unit cell volume as a function of temperature for the $BaCe_{0.65}Zr_{0.20}Y_{0.15}O_{3-\delta}$ sample.

that the overall oxygen stoichiometry for the samples is in the range 2.92−2.94.

Figure 2 shows the evolution of the pseudocubic lattice parameters and of the cell volume as a function of the Zr-content. Overall, all the lattice parameters contract in a linear way along with the Zr-doping without any anisotropic lattice parameter change. It should be mentioned that the Zr-undoped sample has a monoclinic symmetry[30] while the Y-doped barium zirconates have a cubic symmetry.[5]

3.2. Structure Evolution with *T*. All the four samples have been measured up to 800 °C in order to check the structural evolution with temperature. X-ray patterns have been acquired every 20 °C from 40 to 800 °C while neutron diffraction data have been collected every 150−200 °C depending on the sample. In the next sections we are going to present the high-temperature diffraction data for each composition investigated followed by an overall description of the solid solution behavior.

3.2.1. $BaCe_{0.75}Zr_{0.10}Y_{0.15}O_{3-\delta}$. Neutron diffraction patterns (D1A, ILL, Grenoble; λ = 1.9085 Å) collected at selected temperatures are reported in Figure 3. Visual inspection of the data clearly reveals the presence of, at least, three different crystal structures. The monoclinic peak splittings of the RT crystal structure splittings of the crystal structure disappears with increasing temperature leaving a crystal structure that is compatible with an orthorhombic (*Imma*) or a rhombohedral symmetry (within the neutron diffraction resolution; particularly if the orthorhombic distortion is small). We can rule out the presence of the *Pnma* orthorhombic symmetry due to the clear absence of extra-peaks (of significant intensity) found in this space group. At the highest investigated temperature (800 °C), the absence of any reflection around 42° (113) witnesses the setup of a cubic cell.

With this preliminary information obtained from neutron diffraction data, the analysis of the X-ray diffraction patterns have been used to describe how the structure evolves with temperature (thanks to the high density in the *T*-points). As stressed before, the use of both the neutron and X-ray data strongly helped in the reliable definition of the symmetry adopted by the sample.

At RT, $BaCe_{0.75}Zr_{0.10}Y_{0.15}O_{3-\delta}$ has a monoclinic cell. Careful inspection of the patterns suggests that this structure is preserved until about 360 °C. Figure 4 shows some selected regions of the

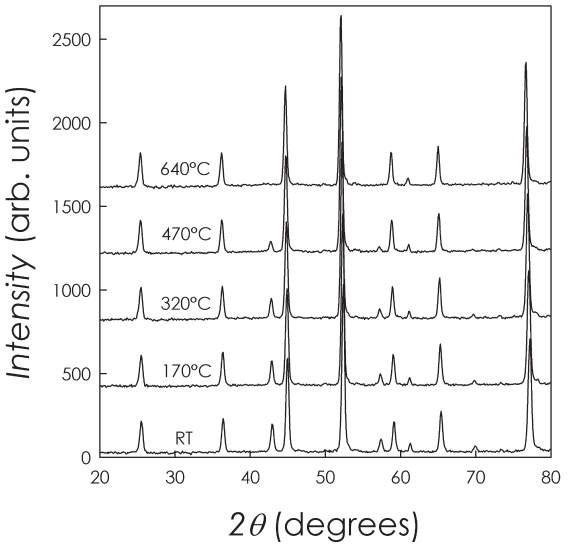

Figure 9. Fragment of the neutron diffraction patterns (HRPT, PSI, λ = 1.494 Å) as a function of temperature collected on the $BaCe_{0.55}Zr_{0.30}Y_{0.15}O_{3-\delta}$ sample.

X-ray patterns (plotted every 40 °C to make the visualization easier). The presence of more than 2 components in the diffraction peaks shown in panels A, B, and C of Figure 4 is only compatible with a perovskite cell of monoclinic symmetry. As stressed above this is in turn confirmed by the neutron data refinement.

At about 380 °C the use of a monoclinic cell leads to a β angle which is 90° within the estimated standard deviation. The actual phase at this temperature has been assessed by a careful analysis of the X-ray patterns. The presence of split peaks like those at about 26° are only compatible with the orthorhombic symmetry which has been identified in the *Imma* cell due to the absence of the extra-reflection found, for example, in the *Pnma* space group. In this case it is not only the high resolution of synchrotron X-ray diffraction which helps in the correct phase identification but also the very high signal/noise ratio which allows the visualization of very low-intensity reflections.

The orthorhombic phase is preserved up to about 640 °C as seen in the change of the asymmetry (Figure 5) in some peculiar

dx.doi.org/10.1021/cm1034326 |*Chem. Mater.* 2011, 23, 1323–1330

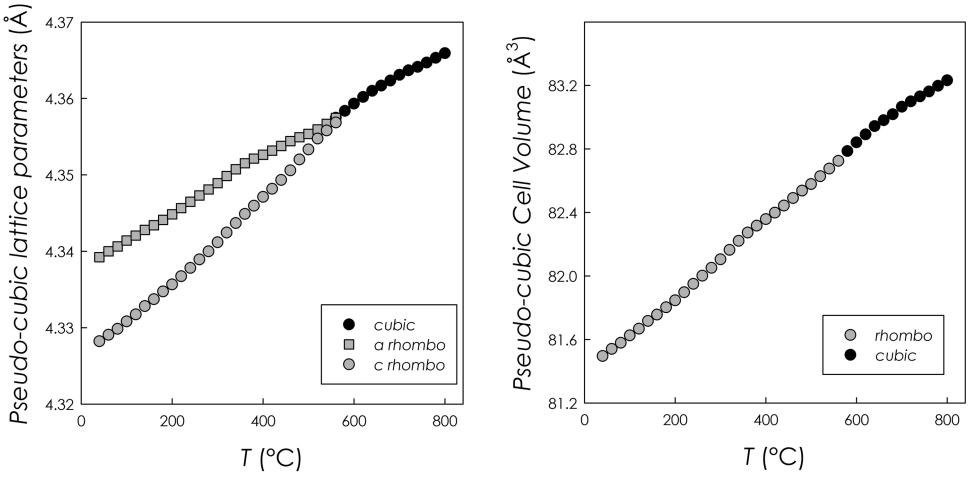

Figure 10. Trend of lattice parameters and unit cell volume as a function of temperature for the $BaCe_{0.55}Zr_{0.30}Y_{0.15}O_{3-\delta}$ sample.

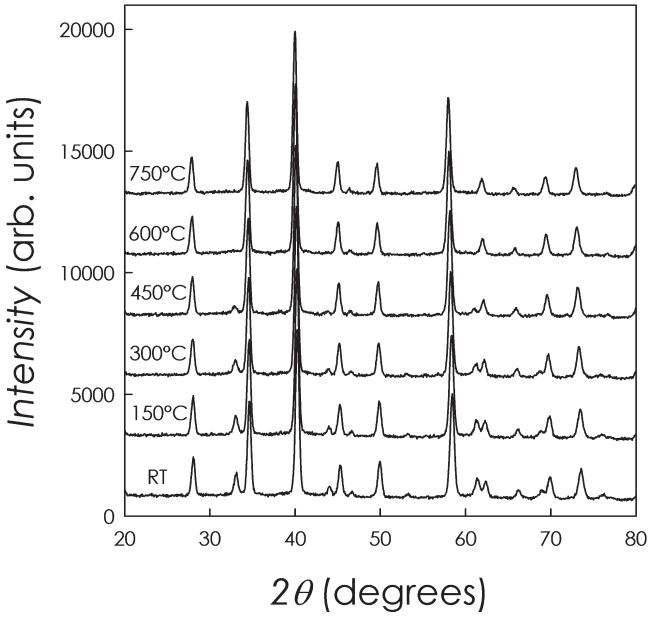

Figure 11. Fragment of the neutron diffraction patterns (HRPT, PSI, λ = 1.494 Å) as a function of temperature collected on the $BaCe_{0.45}Zr_{0.40}Y_{0.15}O_{3-\delta}$ sample.

peaks, and the disappearance of doublets such as the (112) (211) around 21.5° (not shown) which witnesses the setup a rhombohedral symmetry.

Neutron diffraction data reveal that a cubic unit cell is found at 800 °C. Analysis of the X-ray patterns confirm the setup of a cubic symmetry starting from about 700 °C where a clear peak width reduction (indicative of the presence of just one reflection where lower symmetry space groups have two or more) and the disappearance of superlattice reflections typical for the $R\bar{3}c$ space group confirm the presence of a cubic perovskite unit cell. X-ray patterns in selected angular regions (discussed above) are reported in Figure 5 (*T*-step 40 °C). Figure 6 summarizes the trend of lattice parameters and cell volume as determined by the Rietveld refinement of the X-ray diffraction pattern.

3.2.2. $BaCe_{0.65}Zr_{0.20}Y_{0.15}O_{3-\delta}$. Analogous to the x = 0.1 member of the $BaCe_{0.85-x}Zr_xY_{0.15}O_{3-\delta}$ solid solution, neutron and synchrotron X-ray diffraction data as a function of temperature have been collected on the x = 0.2 composition.

Neutron diffraction data (collected on the HRPT instrument at PSI, Villigen; λ = 1.494 Å) at selected temperatures are reported in Figure 7. Refinement of the ND patterns shows that at RT, 150 and 270 °C data are found in the monoclinic symmetry. Data at 450 °C could be quite satisfactorily refined in an orthorhombic or rhombohedral space group but thanks to the X-ray diffraction data it was possible to define the correct unit cell at this temperature as the orthorhombic (*Imma*) one. At 600 °C, $BaCe_{0.65}Zr_{0.20}Y_{0.15}O_{3-\delta}$ is rhombohedral while at 750 °C the unit cell is cubic.

X-ray diffraction analysis of the collected patterns (every 15 °C) allowed to define more precisely the field of existence of each phase for the $BaCe_{0.65}Zr_{0.2}Y_{0.15}O_{3-\delta}$ compound. In details, the crystal structure is (i) monoclinic from RT to 355 °C; (ii) orthorhombic up to 490 °C; (iii) rhombohedral up to 595 °C and finally; (iv) cubic until the highest temperature investigated (800 °C). Figure 8 shows the trend of lattice parameters and unit cell volume as a function of temperature for the $BaCe_{0.65}Zr_{0.20}Y_{0.15}O_{3-\delta}$ as determined from the X-ray diffraction data.

3.2.3. $BaCe_{0.55}Zr_{0.30}Y_{0.15}O_{3-\delta}$. Neutron diffraction patterns as a function of temperature collected on the $BaCe_{0.55}Zr_{0.30}Y_{0.15}O_{3-\delta}$ member of $BaCe_{0.85-x}Zr_xY_{0.15}O_{3-\delta}$ solid solution are reported in Figure 9. All the data up to 470 °C (included) can be nicely refined considering a rhombohedral unit cell while at 640 °C the lattice adopts a cubic symmetry.

Figure 10a,b reports the trend of lattice parameters and unit cell volume as determined from the refinement of the X-ray diffraction patterns. As can be appreciated, the transition temperature from the rhombohedral to the cubic phase falls around 560 °C. As in all the previous cases, no abrupt changes of the cell volume are found at the temperature where the phase transition occurs.

3.2.4. $BaCe_{0.45}Zr_{0.40}Y_{0.15}O_{3-\delta}$. Finally, the neutron data for the x = 0.4 member of $BaCe_{0.85-x}Zr_xY_{0.15}O_{3-\delta}$ solid solution are shown in Figure 11. Also in this case the structure at RT is rhombohedral and keeps this symmetry up to 450 °C even though at this temperature the rhombohedral distortion is already quite small as can be inferred from the intensity of the (113) peak located around 33°.

dx.doi.org/10.1021/cm1034326 |*Chem. Mater.* 2011, 23, 1323–1330

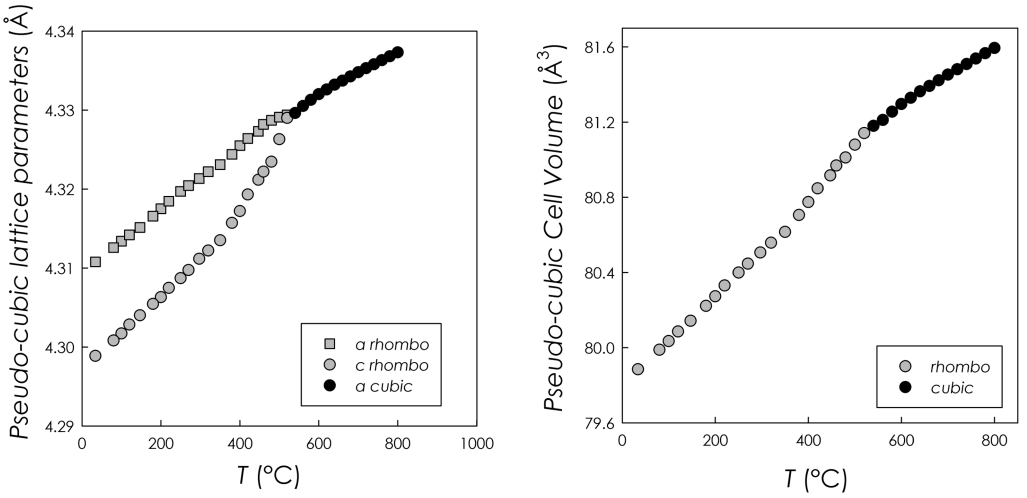

Figure 12. Trend of lattice parameters and unit cell volume as a function of temperature for the $BaCe_{0.45}Zr_{0.40}Y_{0.15}O_{3-\delta}$ sample.

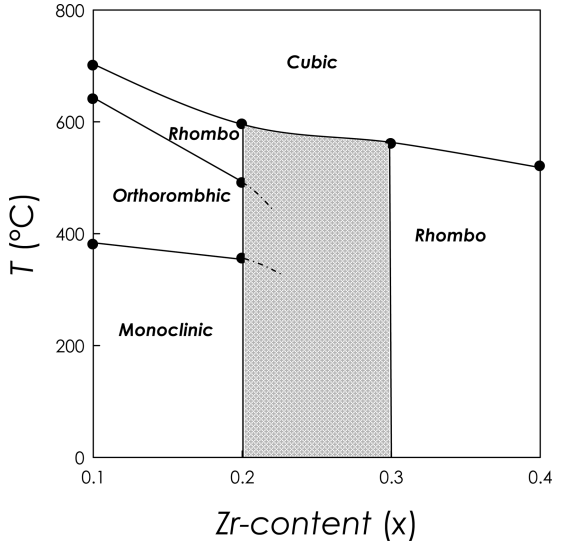

Figure 13. Schematic structural phase diagram for the $BaCe_{0.85-x}Zr_xY_{0.15}O_{3-\delta}$ solid solution.

From the analysis of the synchrotron X-ray diffraction data, we could precisely fix the transition temperature from the rhombohedral to the cubic phase to 520 °C. The trend of the structural parameters are reported in Figure 12.

CONCLUSIONS

In this paper we have investigated the phase stability as a function of temperature of the $BaCe_{0.85-x}Zr_xY_{0.15}O_{3-\delta}$ solid solution for $x = 0.1$, 0.2, 0.3, and 0.4. This system, as mentioned above, is of great interest for the current research on proton conducting oxides since it combines the good water incorporation and solubility performance of Y-doped $BaCeO_3$ with a good chemical stability induced by the Zr-doping. Such electrolytic materials need to be used at relatively high temperatures (above 550−600 °C) in fuel cells devices. As a matter of fact, the knowledge of their crystal structure and phase stability as a function of temperature is essential. By means of combined X-ray synchrotron and neutron diffraction measurements we have provided the phase behavior of selected compositions within the $BaCe_{0.85-x}Zr_xY_{0.15}O_3$ systems.

The diffraction data analysis has shown that the progressive incorporation of Zr within the $BaCe_{0.85}Y_{0.15}O_{3-\delta}$ leads to an increase of symmetry in the crystal structure found at room temperature. Lower doping compositions, i.e., $x = 0.1$ and 0.2, present, as a function of temperature, three successive phase transitions from monoclinic (space group $I2/m$) to orthorhombic ($Imma$), to rhombohedral ($R\bar{3}c$), and finally to the cubic symmetry ($Pm\bar{3}m$). The temperature of these phase transitions reduces as the Zr-content increases, and at $x = 0.3$ and 0.4 only a phase transition from the rhombohedral to the cubic phase occurs. The phase diagram for the $BaCe_{0.85-x}Zr_xY_{0.15}O_{3-\delta}$ solid solution is depicted in Figure 13. The region between $x = 0.2$ and 0.3 has been represented by a dashed area since we actually do not know the fields of existence of the monoclinic and the orthorhombic phases in this composition range. A quite interesting point is that those compositions which are more interesting for application purposes, that is $x = 0.3$ and 0.4 which are chemically stable to CO_2, have quite a symmetric structure and just one phase transition to the cubic phase which in any case does not involve any discontinuity in the volume trend.

Besides the definition of the structural phase diagram of the $BaCe_{0.85-x}Zr_xY_{0.15}O_{3-\delta}$ solid solution, this combined synchrotron and neutron diffraction investigation has clearly revealed that in order to properly characterize the structural features of cerates/zirconates perovskite systems it is necessary to use the high resolution provided by synchrotron radiation but also the advantages of neutron scattering in order to easily distinguish between the different polymorphs.

AUTHOR INFORMATION

Corresponding Author

*Phone: +39-0382-987921. Fax: +39-0382-987575. E-mail: lorenzo.malavasi@unipv.it.

ACKNOWLEDGMENT

This work has been supported by the "INSTM-Regione Lombardia". The ILL and PSI facilities and European Community financial support is acknowledged.

REFERENCES

(1) Malavasi, L.; Fisher, C. A. J.; Islam, M. S. *Chem. Soc. Rev.* **2010**, *39*, 4370–4387.

(2) Steele, B. C. H.; Heinzel, A. *Nature* **2001**, *414*, 345. Goodenough, J. B. *Annu. Rev. Mater. Res.* **2003**, *33*, 91.
(3) Haile, S. M. *Acta Mater.* **2003**, *51*, 5981.
(4) Brett, D. J. L.; Atkinson, A.; Brandon, N. P.; Skinner, S. J. *Chem. Soc. Rev.* **2008**, *37*, 1568.
(5) Orera, A.; Slater, P. R. *Chem. Mater.* **2010**, *22*, 675.
(6) Iwahara, H.; Esaka, T.; Uccida, H.; Maeda, N. *Solid State Ionics* **1981**, *3*−*4*, 359.
(7) Iwahara, H.; Uccida, H.; Ono, K.; Ogaki., J. *J. Electrochem. Soc.* **1988**, *135*, 529.
(8) Yajima, T.; Kazeoka, H.; Yogo, T.; Iwahara, H. *Solid State Ionics* **1991**, *47*, 271.
(9) Yajima, T.; Suzuki, H.; Yogo, T.; Iwahara, H. *Solid State Ionics* **1992**, *51*, 101.
(10) Iwahara, H. *Solid State Ionics* **1992**, *52*, 99.
(11) Iwahara, H.; Yajima, T.; Hibino, T.; Ozaki, K.; Suzuki, H. *Solid State Ionics* **1993**, *61*, 65.
(12) Iwahara, H. *Solid State Ionics* **1996**, *86*−*88*, 9–15.
(13) Katahira, K.; Kohchi, Y.; Shimura, T.; Iwahara, H. *Solid State Ionics* **2000**, *138*, 91.
(14) Ryu, K. H.; Haile, S. M. *Solid State Ionics* **1999**, *125*, 355.
(15) Chiodelli, G.; Malavasi, L.; Tealdi, C.; Barison, S.; Battagliarin, M.; Doubova, L.; Fabrizio, M.; Mortalò, C.; Gerbasi, R. *J. Alloys Comp.* **2009**, *470*, 477.
(16) Kreuer, K. D.; Adams, S.; Munch, W.; Fuchs, A.; Klock, U.; Maier, J. *Solid State Ionics* **2001**, *145*, 295.
(17) Karlsson, M.; Engberg, D.; Bjorketun, M. E.; Matic, A.; Wahnstrom, G.; Sundell, P. G.; Berastegui, P.; Ahmed, I.; Falus, P.; Farago, B.; Bprjesson, L.; Eriksson, S. *Chem. Mater.* **2010**, *22*, 740.
(18) Giannici, F.; Longo, A.; Balerna, A.; Kreuer, K.-D.; Martorana, A. *Chem. Mater.* **2009**, *21*, 2641.
(19) Wu, J.; Davies, R. A.; Islam, M. S.; Haile, S. M. *Chem. Mater.* **2005**, *17*, 846.
(20) Stokes, S. J.; Islam, M. S. *J. Mater. Chem.* **2010**, *20*, 6258.
(21) Azad, A. K.; Irvine, J. T. S. *Chem. Mater.* **2009**, *21*, 215.
(22) Babilo, P.; Uda, T.; Haile, S. M. *J. Mater. Res.* **2007**, *22*, 1322.
(23) Barison, S.; Battagliarin, M.; Cavallin, T.; Doubova, L.; Fabrizio, M.; Mortalò, C.; Boldrini, S.; Malavasi, L.; Gerbasi, R. *J. Mater. Chem.* **2008**, *18*, 5120.
(24) Bjorketun, M. E.; Sundell, P. G.; Wahnstrom, G. *Phys. Rev. B* **2007**, *76*, 054307.
(25) Akbarzadeh, A. R.; Kornev, I.; Malibert, C.; Bellaiche, L.; Kiat, J. M. *Phys. Rev. B* **2005**, *72*, 205104.
(26) Tao, S.; Irvine, J. T. S. *J. Solid State Chem.* **2007**, *180*, 3493.
(27) Zuo, C.; Zha, S.; Liu, M.; Datano, M.; Uchiyama, M. *Adv. Mater.* **2006**, *18*, 3318.
(28) Wu, J.; Li, L. P.; Espinosa, W. T. P.; Haile, S. M. *J. Mater. Res.* **2004**, *19* (8), 2366.
(29) Wang, J. X.; Li, L. P.; Campbell, B. J.; Lv, Z.; Ji, Y.; Xue, Y. F.; Su, W. H. *Mater. Chem. Phys.* **2004**, *86*, 150.
(30) Malavasi, L.; Ritter, C.; Chiodelli, G. *Chem. Mater.* **2008**, *20*, 2343.
(31) Fischer, P.; Frey, G.; Koch, M.; Koknnecke, M.; Pomjakushin, V.; Schefer, J.; Thut, R.; Schlumpf, N.; Burge, R.; Greuter, U.; Bondt, S.; Berruyer, E. *Phys. B* **2000**, *146*, 276.
(32) Rodriguez-Carvajal, J. *Phys. B* **1993**, *192*, 55.
(33) Schmitt, B.; Broennimann, Ch.; Eikenberry, E. F.; Hulsen, G.; Toyokawa, H.; Horisberger, R.; Gozzo, F.; Patterson, B.; Schulze-Briese, C.; Tomikazi, T. *Nucl. Instrum. Methods Phys. Res., Sect. A* **2004**, *518*, 436.
(34) Glazer, A. M. *Acta Crystallogr., Sect. B* **1972**, *28*, 3384.